

Poleward propagation of coupled ENSO fluctuations in atmospheric angular momentum and sea surface temperature

S. I. Marcus & J. O. Dickey

Space Geodetic Science and Applications Group
 Jet Propulsion Laboratory, California Institute of Technology
 4800 Oak Grove Drive, Pasadena, California 91109, USA

Poleward propagation of atmospheric angular momentum (AAM) anomalies, originating on the equator and penetrating to high latitudes in both hemispheres in conjunction with the El Niño/Southern Oscillation (ENSO) phenomenon, was established for the period 1976-1991 by Dickey *et al*. Since atmospheric dissipation times are generally on the order of a month or less, it is natural to suspect that the long-term “memory” for these global-scale fluctuations resides in the ocean. Here we confirm this hypothesis by examining monthly sea-surface temperature (SST) data for the period 1970-1992, obtained from in situ and satellite observations. A high correlation found between AAM anomalies, on the one hand, and thermal wind variations derived from the meridional SST gradient, on the other, demonstrates that the observed propagation pattern results from a coupled ocean-atmosphere response to ENSO.

Interannual variations in AAM, a fundamental measure of the global atmospheric circulation, are strongly linked to the dynamics of ENSO³⁻⁷. Fig. 1 compares a time series of the length-of-day (LOD), an inverse measure of the Earth’s rotation rate which serves as a proxy for global AAM⁸, with the Modified Southern Oscillation Index (MSOI), an

indicator of ENSO activity computed as the difference in sea-level pressure between Darwin and Tahiti. A close relationship between interannual fluctuations in these two quantities is evident, and is statistically significant back to 1930⁷.

Determinations of atmospheric angular momentum, computed from zonal wind data integrated from the surface up to 100 mb, are available from the National Meteorological Center (NMC) beginning in 1976⁹. In our earlier study¹, the clearest propagation pattern emerged by applying a simple one-year minus five-year running mean to the AAM in each latitude belt, which serves as a broad-band interannual filter (having half-power points at 1 1/2 and 8 years) that efficiently removes the annual cycle as well as “decadal” variations from the data. A clear pattern of poleward propagation is evident in the updated Hovmöller diagram (Fig. 2a), with interannual anomalies originating at the equator and propagating to extratropical latitudes in both hemispheres. These results may be verified by using a recursive filter¹⁰ with the same half-power points; a similar pattern is obtained, with less data lost to “window” effects at the beginning and end of the record (Fig. 2b). Westerly anomalies, in particular, are seen to reach their maximum intensity in the sub-tropics, where they are clearly visible during the mature phases of the 1976-77, 1982-83, 1986-87, and 1991-93 ENSO events.

The ENSO phenomenon is bimodal¹¹⁻¹³, with variations falling naturally into a low-frequency (LF) band (- 3-7 years) and a quasi-biennial (QB) band (- 2-3 years). Variations in the LF band, obtained by applying a 32-88 month¹² recursive filter to the AAM data, contain most of the propagating signal (Fig. 2c); the QB band, by contrast, is associated with standing waves in the tropics (visible during the mid- 1980s in Figs. 2ab -- see also Fig. 2c of Dickey *et al.*¹). The robustness of the LF propagation is further confirmed by examining a “consensus” hindcast for the decade 1979-1988, formed by averaging the results of 13 GCM simulations carried out as part of the Atmospheric Model Intercomparison Project¹⁴; the corresponding Hovmöller diagram (Fig. 2d) shows a clear pattern of poleward propagation associated with the 1982-83 and 1986-87 ENSOs.

Poleward propagation of AAM in association with ENSO has also been noted by Salstein *et al.*¹⁵ in a multi-decade rawinsonde-based data set compiled by Oort¹⁶.

What is the origin of these long-lived, globally coherent circulation anomalies? Especially in view of their connection with ENSO, the most likely mechanism involves the large-scale sea-surface temperature (SST) variations which characterize that phenomenon. In order to investigate this hypothesis, monthly SST data were obtained on a $2^\circ \times 2^\circ$ grid for the period January 1970–December 1992 from the Climate Analysis Center². For January 1970–December 1981 the data were derived exclusively from in situ measurements with coverage from 60°N to 40°S , while for January 1982–December 1992 satellite data were included to form a blended analysis with global coverage. For comparison with the AAM data, the monthly SST values were zonally averaged and binned into 46 equal-area latitude belts. Monthly values of the thermal wind, a measure of the vertical wind shear required to maintain geostrophic and hydrostatic balance in the presence of a meridional temperature gradient¹⁷, were also computed from the zonally-averaged SST data.

Although the strongest El Niño warming occurs in the eastern tropical Pacific¹⁸, the ENSO cycle also has a clear signature in the record of zonally-averaged equatorial SST (Fig. 3a). Poleward propagation of zonally-averaged SST filtered in the LF band (Fig. 3b) is evident for the two ENSO events having the largest equatorial anomalies (1972-73 and 1986-87), while the very strong¹⁹ 1982-83 event, for which the zonal-mean SST anomaly in the LF band was actually smaller, showed robust propagation in the SH with a weaker signature in the NH. By contrast the 1976-77 ENSO exhibits only a weak maximum in zonally-averaged SST at the equator, and is characterized by a disorganized propagation pattern. The 1976-77 event was somewhat anomalous, with ENSO-like signals in some indices and none in others (see Enfield²⁰ and references therein); note in particular the double peak in LOD surrounding this event (Fig. 1). The thermal wind field also shows a clear pattern of poleward propagation in the LF band with the exception of the 1976-77

event (Fig. 3c); in particular, the initial stages of the 1991-93 ENSO are visible, although a longer time series is needed to trace its full development.

Meridional propagation of geophysical quantities maybe conveniently summarized by means of latitude-lag correlation diagrams²¹. Figs. 4a-b plot the correlation between latitudes 60°N and 40°S of LF-filtered variations in AAM and SST, respectively, with the average of the corresponding variable in the two latitude belts straddling the equator. Both plots show a clear tendency for propagation of zonally-averaged anomalies from the equator to the extratropics. The SST propagation pattern is more robust in the tropics, with the strongest negative correlations distributed symmetrically in time (at a lag/lead of 2 years) along the equator. By contrast the AAM pattern shows the largest negative correlation in the sub-tropics at a lead of 6-12 months, indicating that the strong AAM variations occurring in this region may help to set the stage for the onset of the opposite phase of ENSO at the equator.

Cross-correlation diagrams (Figs, 4c-d) summarize the relationship between zonally-averaged anomalies in the AAM and SST data during their period of overlap (1976-1992), LF-filtered variations in these two quantities are in quadrature with each other at most latitudes (Fig. 4c), with the strongest correlations found at a lag/lead of about one year. The correlation of AAM with the SST-derived thermal wind forcing (Fig. 4d), however, shows a strong, nearly simultaneous relationship in the LF band at most latitudes except near the equator (where the thermal wind relationship is not valid), confirming that the global propagation of interannual AAM anomalies is dynamically linked to similar variations in the underlying SST field.

The meridional propagation of SST anomalies may, in turn, be related to heat transport within the oceans themselves. Wyrtki²², for example, showed that the export of warm water from the tropics plays a key role in the dynamics of the ENSO cycle, while Miller and Cheney²³ used Geosat data to document the transport of warm water across latitude 80N during the 1986-87 El Niño, and Chao and Philander²⁴ found large

interannual variations in heat transport across 60N in an oceanic general circulation model forced with observed monthly winds for the period 1967 to 1979. More recently, White²⁵ has documented the poleward propagation of slow ENSO waves in upper layer heat content to high latitudes along the eastern boundaries of the North Pacific, North Atlantic, and South Indian oceans.

The occurrence of interannual fluctuations in oceanic heat transport, linked to poleward-propagating AAM variations through the meridional SST gradient, may also reflect the presence of coupled modes in the ocean-atmosphere system. The fastest-growing mode in the years-decades oscillation range of a zonally-symmetric, global ocean-atmosphere model due to Mehta²⁶, for example, is characterized by strong SST anomalies near the equator, which subsequently propagate to higher latitudes. Since the zonally-averaged equatorial SST shows pronounced variability associated with El Niño (Fig. 3a), the (asymmetrically-forced) ENSO cycle has a strong projection on this mode, whose growth in the real ocean-atmosphere system maybe limited by the lack of zonal symmetry. Our results suggest that a similar coupled mode, arising as a forced response to the zonally-symmetric component of ENSO heating at the equator, maybe responsible for the global-scale propagation of atmospheric and oceanic anomalies summarized in this report.

References

1. Dickey, J. O., Marcus, S. L., & Hide, R. *Nature* 357,484-488 (1992).
2. Reynolds, R. W. personal communication (1993).
3. Rosen, R. D., Salstein, D. A., Eubanks, T. M., Dickey, J. O., & Steppe, J. A. *Science* 225,411-414 (1984).
4. Eubanks, T. M., Steppe, J. A., & Dickey, J. O. in *Earth Rotation: Solved and Unsolved Problems* (ed. Cazenave, A.) 163-186 (Reidel, Hingham, Massachusetts 1986).
5. Chao, B. F. *J. Geophys. Res.* 93, 7709-7715 (1988).
6. Chao, B. F. *Science* 243, 923-925 (1989).
7. Dickey, J. O., Marcus, S. L., Hide, R., & Eubanks, T. M. in *American Geophysical Union Monograph, Interactions between Global Climate Subsystems: The Legacy of Harm* (eds. McBean, G. A., & Mantel, M.) 141-155, 1993.
8. Hide, R., & Dickey, J. O. *Science* 253, 629-637 (1991).
9. Salstein, D. A., Kann, D. M., Miller, A. J., & Rosen, R. D. *Bull. Amer. Meteor. Soc.* 74, 67-80 (1993).
10. Murakami, M. *J. Geophys. Res.* 97, 994-1013 (1979).
11. Rasmussen, E. V., Wang, X., & Ropelewski, C. F. *J. Mar. Systems* 1, 71-96 (1990).
12. Barnett, T. P., *J. Clim.* 4, 269-288 (1991).
13. Keppenne, C. L., & Ghil, M. *J. Geophys. Res.* 97, 20449-20454 (1992).
14. Marcus, S. L., & Dickey, J. O. in *Sixth Conference on Climate Variations*, 70-74 (American Meteorological Society, Boston, Massachusetts 1994).
15. Salstein, D. A., Black, R. X., & Rosen, R. D. in *Fourth Symposium on Global Change Studies*, 331 -334 (American Meteorological Society, Boston, Massachusetts 1993).

16. Oort, A. H., *NOAA Professional Paper 14*, U. S. Dept. of Commerce (1983).
17. Gill, A. E. *Atmosphere-Ocean Dynamics* (Academic Press, New York 1982)..
18. Philander, S. G. H. *El Niño, La Niña and the Southern Oscillation* (Academic Press, New York, 1990).
19. Quinn, W. H., & Neal, V. T. *J. Geophys. Res.* 92, 14449-14461 (1987).
20. Enfield, D. B. *Rev. Geophys.* 27, 159-187 (1989).
21. Risbey, J. S., & Stone, P. H. *J. Atmos. Sci.* 45, 2026-2038 (1988).
22. Wyrtki, K. *J. Geophys. Res.* 90, 7129-7132 (1985).
23. Miller, L., & Cheney, R. *J. Geophys. Res.* 95, 17905-17919 (1990).
24. Chao, Y., & Philander, S. G. H. *J. Clim.* 6, 450-469 (1993).
25. White, W. B. *J. Geophys. Res.*, manuscript submitted.
26. Mehta, V. M. *J. Clim.* 5, 330-342 (1992).

Acknowledgements: Valuable comments regarding the work presented here were made by R. Hide and R. Gross. The authors thank D. A. Salstein and R. D. Rosen for providing the AAM data set, and R. W. Richards for providing the gridded SST data used in the analysis. The work of the authors presents the results of one phase of research carried out at the Jet Propulsion Laboratory, California Institute of Technology, under contract with the National Aeronautics and Space Administration.

Figure Legends

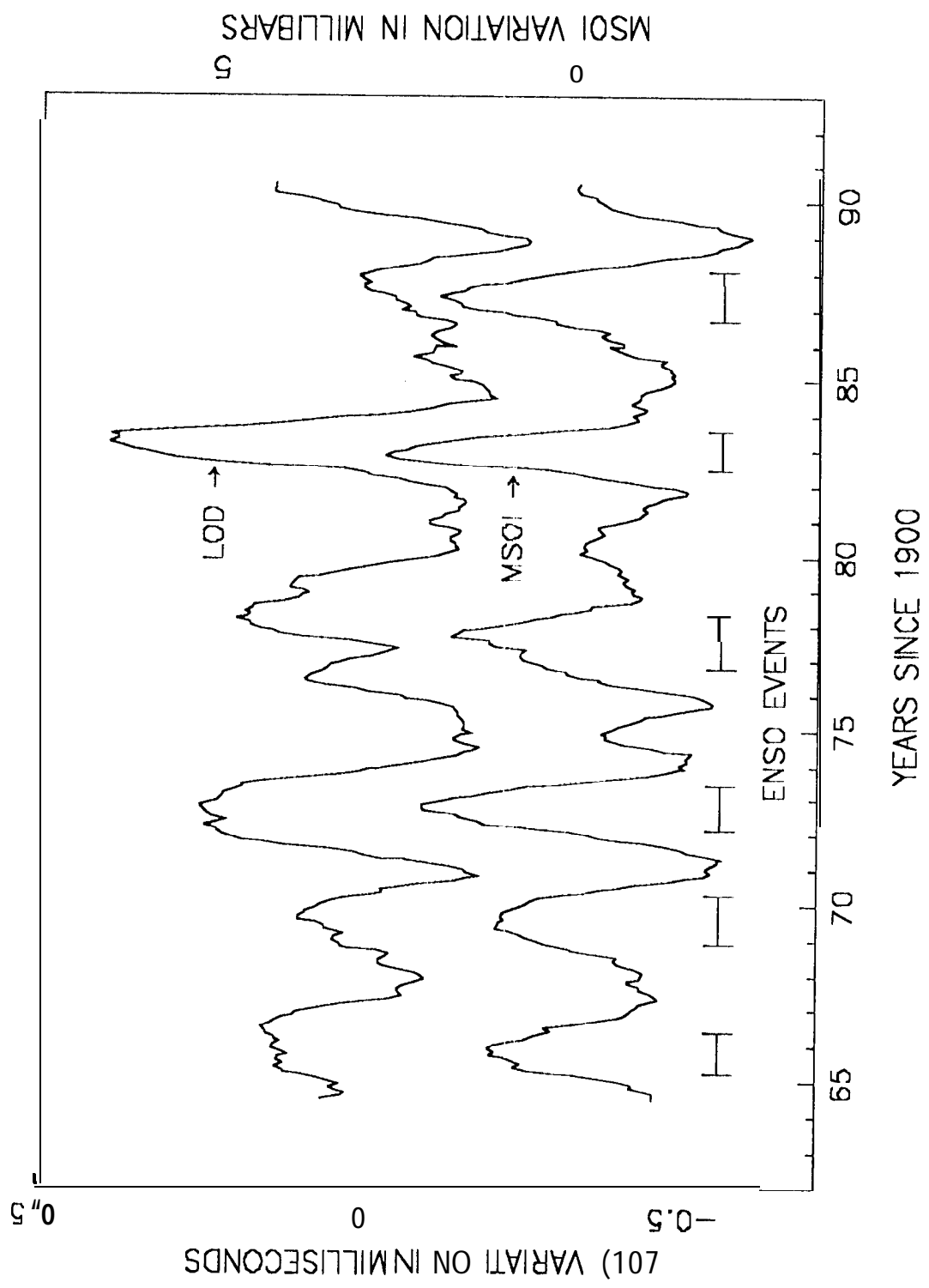
FIG. 1 Interannual variations in length-of-day (LOD) and the Modified Southern Oscillation Index (MSOI), computed as the difference between one-year and five-year running averages (an arbitrary vertical offset is used for clarity). Warm ENSO events occur when the MSOI, defined as the surface pressure difference between Darwin and Tahiti, becomes anomalously high. These events are also marked by positive interannual fluctuations in LOD, which indicate a slowing of the Earth's rotation and therefore (since the atmosphere and Earth form a closed dynamical system) an increase in the axial angular momentum of the atmosphere.


FIG. 2 Hovmöller (time-latitude) diagrams of atmospheric angular momentum, computed from zonally-averaged zonal winds integrated from the surface to the 100 mb level, in 46 equal-area latitude belts⁹ numbered from north to south. *a*, Interannual variation obtained from the difference between one-year and five-year moving averages in each latitude belt (the first and last 2 1/2 years of data are truncated); *b*, obtained by applying a recursive filter with half-power points at 18 and 96 months to the data in each latitude belt; *c*, the low-frequency (LF) component obtained by applying a 32-88 month recursive filter in each latitude belt; *d*, obtained by applying an LF filter to a "consensus" hindcast for the decade 1979-1988, formed by averaging the results of 13 GCM simulations carried out as part of the Atmospheric Model Intercomparison Project.

FIG. 3 *a*, Average of zonal-mean sea-surface temperature (SST) in the two latitude belts straddling the equator (blue curve); a trend and mean seasonal cycle have been removed from the data. The LF component, obtained by recursive filtering in the 32-88 month band, is also shown (red curve). *b*, Hovmöller (time-latitude) plot of zonally-averaged SST data, filtered in the LF band in each of 46 equal-area latitude belts; before 1982, data coverage is limited to the region 600N-400S (see text). *c*, Hovmöller plot of LF-filtered thermal wind data, derived from the meridional SST gradient (the absolute value of the Coriolis

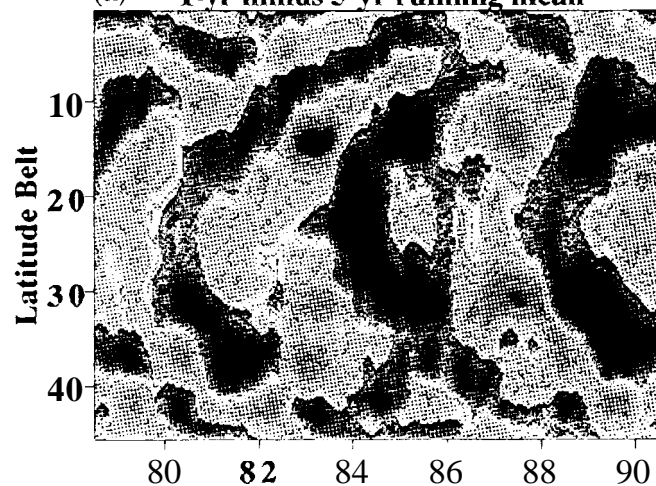
parameter was bounded from below by its value at 20° latitude to avoid excessive values of the computed thermal wind in the tropics).


FIG. 4a, Correlation coefficient between LF-filtered AAM variations in latitude belts from 4 to 38 (60°N - 40°S) with the average of the LF-filtered AAM in the two latitude belts straddling the equator, using data from the period 1976-1992. The standard deviation of the correlation coefficient was computed using a pooled estimate of the variance from all latitudes. *b*, As in *a*, for zonally-averaged SST data from the period 1970-1992, *c*, Correlation coefficient between LF-filtered AAM and SST variations in latitude belts from 4 to 38, for the period 1976-1992. *d*, as in *c*, for the correlation between AAM and thermal wind variations derived from the meridional SST gradient.



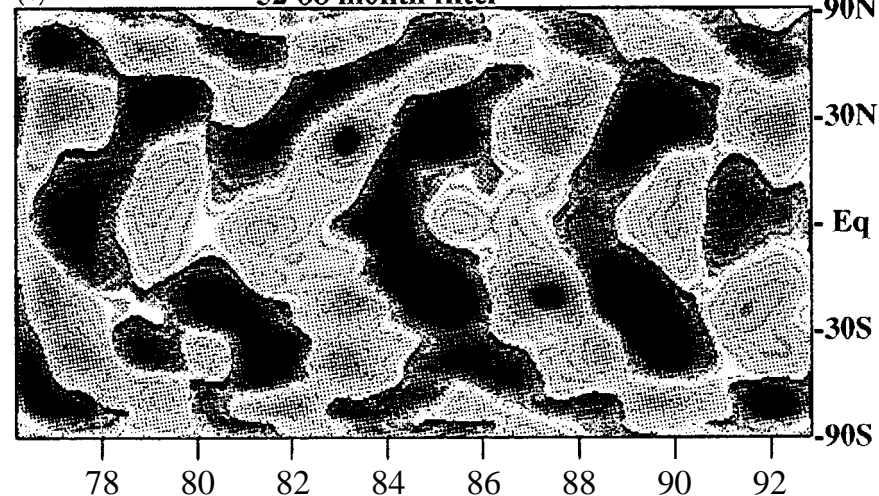
Easterly  *Westerly*
 $10^{24} \text{ kg m}^2 \text{ sec}^{-1}$

(a) 1-yr minus 5-yr running mean

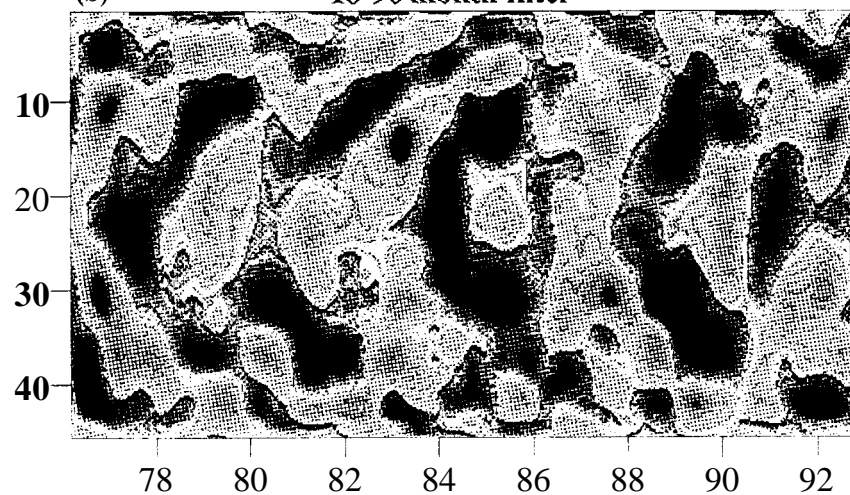


 *Westerly*
 $10^{24} \text{ kg m}^2 \text{ sec}^{-1}$

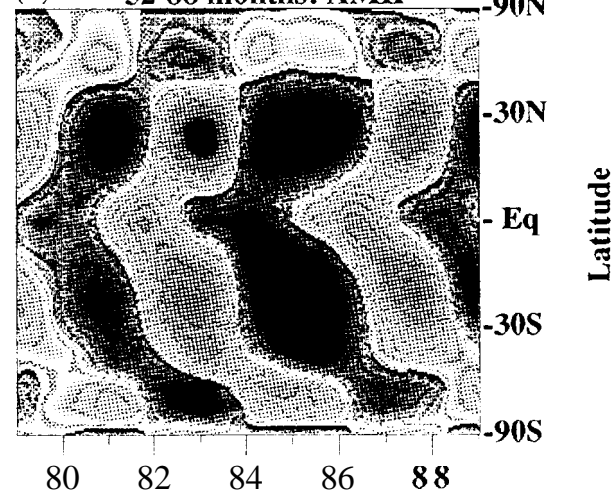
(c) 32-88 month filter



(b) 18-96 month filter

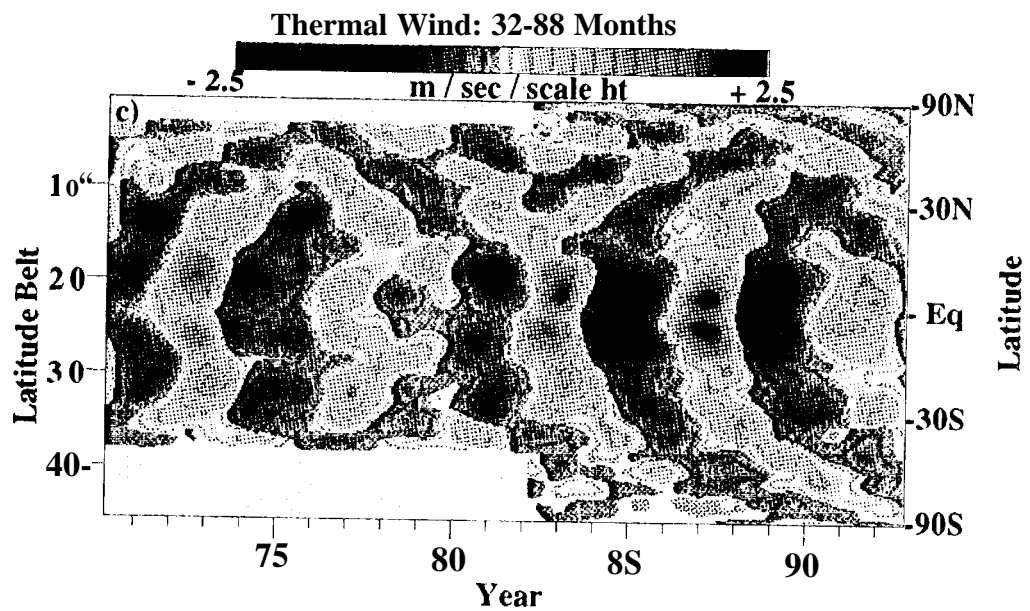
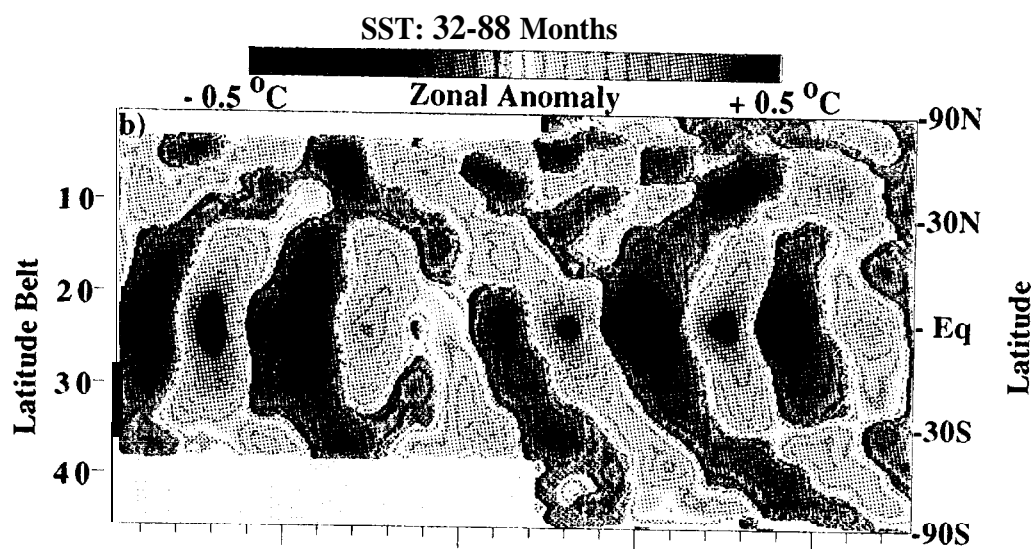
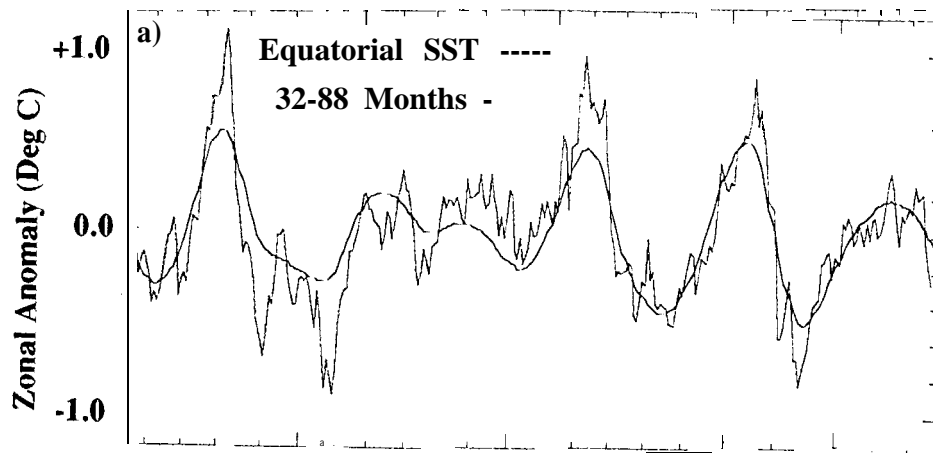


(d) 32-88 months: AMIP

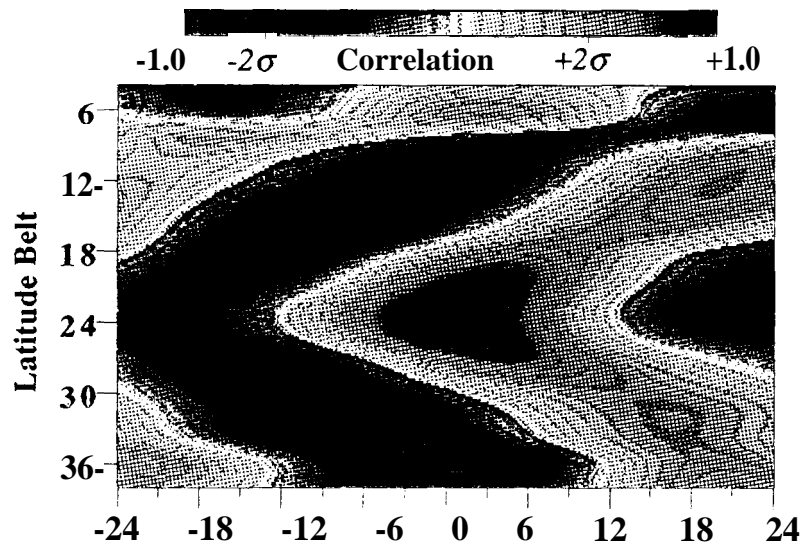


Years Since 1900

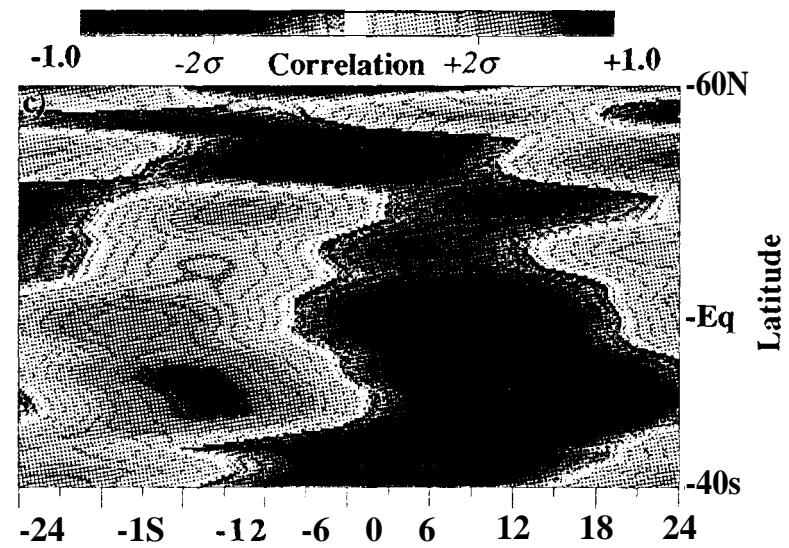
Years Since 1900



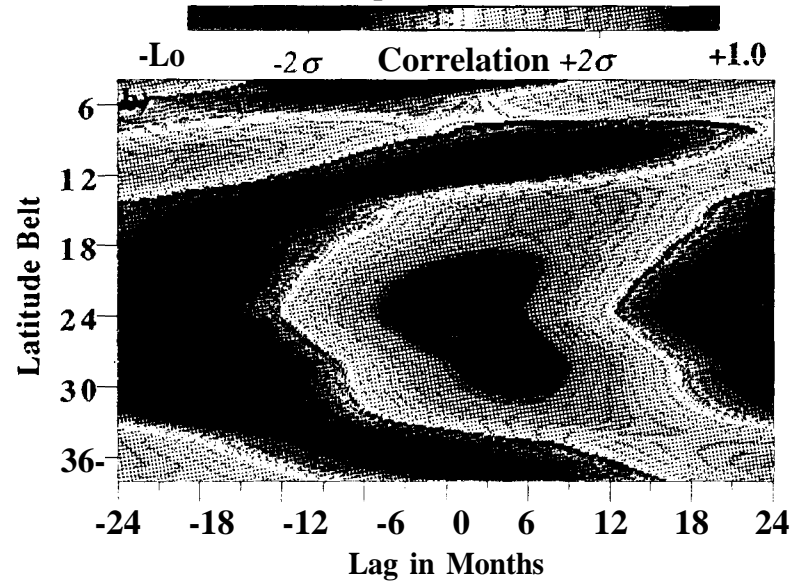
AAM vs Eq. AAM: 32-88 Months



AAM vs SST: 32-88 Months



SST vs Eq. SST: 32-88 Months



AAM vs Thermal Wind: 32-88 Months

